Multiplicity of X-ray selected T Tauri stars in the Scorpius-Centaurus OB association[*]

R. Köhler[1,2], M. Kunkel[2], C. Leinert[2], and H. Zinnecker[1]

[1] Astrophysikalisches Institut Potsdam, An der Sternwarte 16, 14482 Potsdam, Germany
[2] Max-Planck-Institut für Astronomie, Königstuhl 17, 69117 Heidelberg, Germany

Abstract. We report the results of a search for binarity among young stars, performed in the Scorpius-Centaurus OB association on a sample of 118 X-ray selected T Tauri stars. We use speckle interferometry and direct-imaging observations to find companions in the separation range $0.13'' - 6''$. After corrections to account for confusion with background stars and for the bias induced by the X-ray selection, we find a multiplicity (number of binaries or multiples divided by number of systems) of (32.6 ± 6.1) %, and a number of companions per system of (35.2 ± 6.3) %. This is higher by a factor of 1.59 ± 0.34 compared to main-sequence stars, but slightly lower than in a sample in the Taurus-Auriga star-forming region that was selected and studied similarly. In Scorpius-Centaurus, we find fewer binaries with nearly equal brightness than in Taurus-Auriga. There are significant differences between the period distributions in the two subgroups Upper Scorpius A and B: The peak of the distribution of stars in US-A is at about 10^5 days, while that of stars in US-B is around $10^{6.5}$ days. We compared our results with the optical multiplicity survey of Brandner et al. (1996), whose sample contains 49 stars that were also observed by us, and find no infrared companions. The flux ratio distributions of close and wide binaries in our sample show no significant difference.

Key words: stars: pre-main sequence – stars: binaries: visual – infrared: stars – surveys – techniques: interferometric

1. Introduction

The determination of the binary frequency of young low-mass stars born in different star formation environments remains an important observational goal. For example, it remains to be seen whether the multiplicity of T Tauri stars in OB associations differs from that in T associations, and also whether the multiplicity in associations is significantly different from that in young clusters. The interest in these generic differences stems from the fact that the endproduct of star formation (stellar masses and stellar multiplicity, including mass ratios and semi-major axis distributions of the components) may depend on the initial conditions

and on the density of clustering (mean neighbour separation) in the star forming region.

In particular, the binary frequency in OB associations like Scorpius-Centaurus is of interest because it is unclear if it is as high as that of loose T associations like Taurus-Auriga (Leinert et al. 1993, Ghez et al. 1993, Köhler & Leinert 1998) or as low as that of dense clusters like the Pleiades (Bouvier et al. 1997), the Hyades (Patience et al. 1998), or the Orion Trapezium Cluster (Prosser et al. 1994, Padgett et al. 1997, Petr et al. 1998, Simon et al. 1999). This should reflect whether OB associations were originally dense concentrations of stars that expanded quickly after the residual gas was dispersed, or whether OB associations were actually loose systems at birth, like T associations, the only difference being their size and stellar content.

There is yet another reason for our interest in the binary frequency of a representative OB association. According to Miller and Scalo (1978), OB associations should be the dominant birthplace of low-mass field stars, if the Initial Mass Function (IMF) in OB associations is similar to the field star IMF. There are now indications that this is indeed the case (Preibisch & Zinnecker 1999). This implies that we would expect the binary frequency of low-mass stars in OB associations to be roughly the same as the binary frequency of field stars (Duquennoy & Mayor 1991). By comparing the results of multiplicity surveys of young stars in different star-forming environments to those of main-sequence stars, one can constrain what the dominant mode of low-mass star-formation is ("inverse dynamical population synthesis", Kroupa 1995).

Scorpius-Centaurus is well suited for a multiplicity survey, since it is the most nearby OB association, located at a distance of about $145\,\mathrm{pc}$ (de Zeeuw et al. 1999). Furthermore, we can base our work on the surveys of Walter et al. (1994, hereafter W94) and Kunkel (Kunkel 1999, hereafter K99, Kunkel et al. 2000), who identified in total 121 T Tauri stars with the help of spectroscopic follow-up observations of X-ray sources detected by the EINSTEIN and ROSAT satellites, respectively.

2. The sample

Our object list was compiled from two sources: the work of Walter et al. (1994) and the PhD thesis of Michael Kunkel (1999, Kunkel et al. 2000).
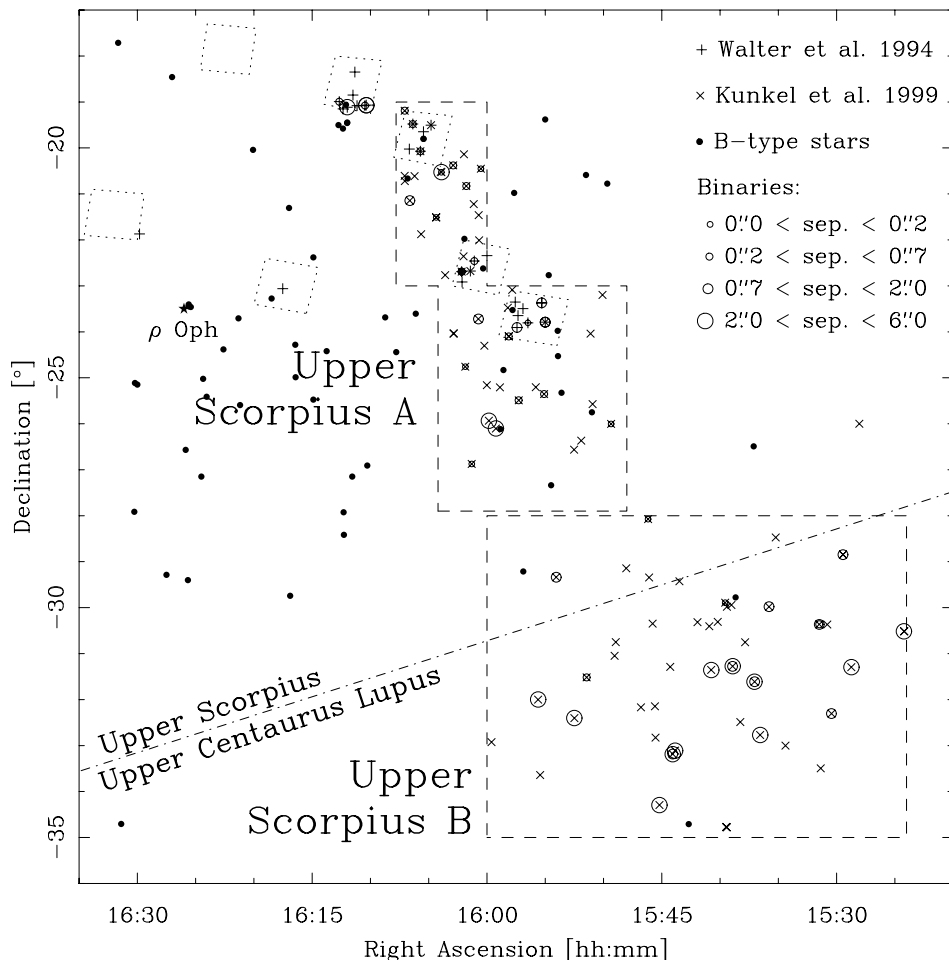

Fig. 1. Spatial distribution of the stars in our sample. The regions observed by EINSTEIN are outlined by dotted lines. The regions outlined by dashed lines mark the area where K99 carried out follow-up observations of ROSAT sources. We divide this area in two sub-regions designated Upper Scorpius A and B (see Sect. 5.4). The dash-dotted line marks the boundary between Upper Scorpius and Upper Centaurus Lupus as defined by de Zeeuw et al. (1998).

Walter et al. (1994) searched for PMS objects among X-ray sources discovered by the EINSTEIN satellite. EINSTEIN observed seven fields in Scorpius-Centaurus, these are indicated in Fig. 1. Walter et al. (1994) identified 28 T Tauri stars within these fields based on their spectral type and the lithium absorption line at 6707 Å.

Michael Kunkel used the Simbad database, the Hubble GSC, and POSS plates to search for optical counterparts within the error circles of X-ray sources found in the ROSAT All-Sky Survey (RASS) and with pointed ROSAT observations. Candidates for T Tauri stars (down to a magnitude of B $\approx$ 17$^{\rm m}$) were observed spectroscopically. Again, the Li absorption line was used to identify young stars. The area studied has the following coordinates (see also Fig. 1):

— 15$^{\rm h}$ 24$^{\rm m}$ to 16$^{\rm h}$ 00$^{\rm m}$, $-35°$ to $-28°$,
— 15$^{\rm h}$ 48$^{\rm m}$ to 16$^{\rm h}$ 04$^{\rm m}$, $-28°$ to $-23°$,
— 16$^{\rm h}$ 00$^{\rm m}$ to 16$^{\rm h}$ 08$^{\rm m}$, $-23°$ to $-19°$.

In total, 99 T Tauri stars were found, 94 weak-line T Tauri stars (WTTS) and 5 classical T Tauri stars (CTTS). Most of these sources were discovered in the RASS; however, 13 of them could only be detected with pointed ROSAT observations. Table 1 lists the 99 stars, their positions and other parameters that are important for our survey.

Since both of these studies refer to the same association, and since both use spectroscopic confirmation of X-ray selected candidates with similar sensitivities, we combine these two object lists into a larger sample. In Sect. 5.1 we will give further justification for this decision. Six stars were found both by W94 and by K99. Three pairs of stars (RXJ 1537.0-3136 A+B, RXJ 1540.7-3121 A+B, and RXJ 1552.5-3224 A+B) are separated by less than 6$''$, therefore we count them as binaries.

Our multiplicity survey is hence based on a list of 118 systems, where "system" means either a single star, a binary, or a multiple. The positions of these stars are plotted in Fig. 1, the complete object lists with additional data can be found in W94 and K99.

3. Observations and data analysis

The speckle observations were carried out at the ESO New Technology Telescope (NTT) on La Silla, Chile, in May 1994 and July 1995. We used the SHARP camera (System for High Angular Resolution Pictures) of the Max-Planck-Institut for Extraterrestrial Physics (Hofmann et al. 1992). All observations were performed in the K-band at 2.2 μm.

Although speckle interferometry can be considered by now a standard technique (Leinert 1992), no program for speckle

Table 1. The object list of Kunkel (1999). The first column gives a running number, the second gives the official designation of the star, the third to fifth column give the coordinates and the number of counts ROSAT detected from this star. The last three columns specify whether the star was found in the RASS and/or a pointed observation, its spectral type and the subregion where the star is located (see Fig. 1)

No.	Designation	α_{2000}	δ_{2000}	X-ray counts[1]	RASS/pnt.	Sp. type	Region
1	RX J1524.2-3030A	15:24:11.5	-30:30:57	11.7	S	K0	US-B
2	RX J1524.2-3030B	15:24:13.0	-30:30:55	11.7	S	M1	US-B
3	RX J1528.0-2600	15:28:03.2	-26:00:02	19.1	S	K3	US-B
4	RX J1528.7-3117	15:28:43.9	-31:17:39	95.9	S	G8	US-B
5	RX J1529.4-2850A	15:29:26.9	-28:50:51	62.9	S	G8	US-B
6	RX J1529.4-2850B	15:29:26.9	-28:50:51	62.9	S	G6	US-B
7	RX J1530.4-3218	15:30:26.2	-32:18:11	386.3	S	G7	US-B
8	RX J1530.8-3021	15:30:47.9	-30:22:04	14.1	S	K2	US-B
9	RX J1531.3-3329	15:31:21.9	-33:29:39	47.2	S	G8	US-B
10	RX J1531.5-3021	15:31:29.6	-30:21:53	13.2	S	M0	US-B
11	RX J1534.3-3300	15:34:23.1	-33:00:07	25.5	S	M0	US-B
12	RX J1535.2-2828	15:35:13.5	-28:28:26	27.7	S	G0	US-B
13	RX J1535.8-2958	15:35:48.3	-29:58:54	19.7	S	M4	US-B
14	RX J1536.5-3246	15:36:33.7	-32:46:10	14.3	S	M3	US-B
15	RX J1537.0-3136A	15:37:02.0	-31:36:38	703.2	S/P	G7	US-B
16	RX J1537.0-3136B	15:37:02.0	-31:36:38	703.2	S/P	K7	US-B
17	RX J1537.8-3045	15:37:51.3	-30:45:15	136.6	S/P	K4	US-B
18	RX J1538.2-3229	15:38:16.1	-32:29:22	46.1	P	G3	US-B
19	RX J1538.9-3116	15:38:55.2	-31:16:31	66.7	P	M2	US-B
20	RX J1539.0-2956	15:39:01.8	-29:56:30	50.5	P	K4	US-B
21	RX J1539.4-2958	15:39:25.0	-29:58:44	61.9	S/P	M2	US-B
22	RX J1539.4-3446A	15:39:25.2	-34:46:49	14.4	S	G1	US-B
23	RX J1539.4-3446B	15:39:27.6	-34:46:16	14.4	S	K7	US-B
24	RX J1539.4-3446C	15:39:28.2	-34:46:17	14.4	S	M2	US-B
25	RX J1539.5-2953	15:39:33.8	-29:53:30	21.0	P	M3	US-B
26	RX J1540.2-3018	15:40:12.2	-30:18:30	21.8	P	M3	US-B
27	RX J1540.7-3121A	15:40:45.6	-31:21:12	21.6	S/P	M4	US-B
28	RX J1540.7-3121B	15:40:45.6	-31:21:12	21.6	S/P	M5	US-B
29	RX J1540.9-3024	15:40:55.4	-30:24:18	81.3	S/P	M2	US-B
30	RX J1541.9-3019	15:41:56.2	-30:19:00	79.3	P	M4	US-B
31	RX J1543.4-2925	15:43:29.2	-29:25:34	13.4	S	K0	US-B
32	RX J1543.8-3306	15:43:51.6	-33:06:28	94.8	S	M3	US-B
33	RX J1544.0-3311	15:44:03.6	-33:11:11	43.0	S	G9	US-B
34	RX J1544.2-3117	15:44:16.6	-31:17:12	19.6	P	G3	US-B
35	RX J1545.2-3417	15:45:12.0	-34:17:30	79.1	S	K0	US-B
36	RX J1545.5-3249	15:45:32.1	-32:49:36	< 13.3	S	G9	US-B
37	RX J1545.6-3208	15:45:35.3	-32:08:49	< 10.5	S	K3	US-B
38	RX J1545.8-3020	15:45:47.6	-30:20:52	3028.9	S/P	K3	US-B
39	RX J1546.0-2920	15:46:05.5	-29:20:40	< 13.1	S	M0	US-B
40	RX J1546.1-2804	15:46:10.8	-28:04:22	39.6	S	G9	US-B
41	RX J1546.7-3210	15:46:47.0	-32:10:06	54.7	P	M2	US-B
42	RX J1548.0-2908	15:48:02.9	-29:08:36	36.4	S	G9	US-B
43	RX J1548.9-3045	15:48:57.1	-30:45:00	44.8	P	M2	US-B
44	RX J1549.0-3102	15:49:02.7	-31:02:52	652.6	S/P	K0	US-B
45	RX J1549.3-2600	15:49:21.0	-26:00:05	56.5	S	K0	US-A
46	RX J1550.0-2312	15:50:05.0	-23:11:53	< 11.1	S	M2	US-A
47	RX J1550.9-2534	15:50:56.4	-25:34:18	23.2	S	F9	US-A
48	RX J1551.1-2402	15:51:06.6	-24:02:19	33.2	S	M2	US-A
49	RX J1551.4-3131	15:51:26.8	-31:30:59	9.5	S	M1	US-B

[1]: In cases where more than one star was found within the error box of one X-ray source, we divided the X-ray counts equally among them

Table 1. (continued)

No.	Designation	α_{2000}	δ_{2000}	X-ray counts[1]	RASS/pnt.	Sp. type	Region
50	RX J1551.9-2621	15:51:54.4	-26:22:04	78.6	S	G0	US-A
51	RX J1552.5-3224A	15:52:30.0	-32:24:12	15.0	S	M2	US-B
52	RX J1552.5-3224B	15:52:30.0	-32:24:12	15.0	S	M3	US-B
53	RX J1552.5-2633	15:52:31.3	-26:33:51	11.8	S	M0	US-A
54	RX J1554.0-2920	15:54:03.6	-29:20:15	23.8	S	M0	US-B
55	RX J1554.9-2347[2]	15:54:59.9	-23:47:18	3750.7	S/P	G2	US-A
56	RX J1555.1-2521	15:55:06.2	-25:21:09	303.6	S/P	M1	US-A
57	RX J1555.4-3338	15:55:26.2	-33:38:23	19.9	S	K5	US-B
58	RX J1555.6-3159	15:55:37.0	-31:59:58	12.4	S	M2	US-B
59	RX J1555.8-2512	15:55:48.8	-25:12:23	423.1	S/P	G3	US-A
60	RX J1557.3-2529	15:57:16.7	-25:29:18	93.7	P	M0	US-A
61	RX J1557.8-2305	15:57:50.0	-23:05:09	29.1	S	M0	US-A
62	RX J1558.1-2405B	15:58:07.4	-24:05:54	28.5	P	M5	US-A
63	RX J1558.1-2405A	15:58:08.2	-24:05:52	28.5	P	K4	US-A
64	RX J1558.2-2328	15:58:12.7	-23:28:36	317.5	S/P	G2	US-A
65	RX J1558.8-2512	15:58:53.6	-25:12:32	86.0	P	M1	US-A
66	RX J1559.2-2606	15:59:14.5	-26:06:18	12.7	S	K2	US-A
67	RX J1559.6-3255	15:59:36.7	-32:55:36	22.4	S	G8	US-B
68	RX J1559.8-2556	15:59:50.1	-25:55:58	15.3	S	M2	US-A
69	RX J1600.0-2509	16:00:00.8	-25:09:42	286.5	S/P	G0	US-A
70	RX J1600.2-2417	16:00:13.3	-24:18:10	< 30.9	P	M0	US-A
71	RX J1600.5-2027	16:00:31.4	-20:27:05	37.4	S	M1	US-A
72	RX J1600.6-2159	16:00:40.6	-22:00:32	19.3	S	G9	US-A
73	RX J1600.7-2127	16:00:42.8	-21:27:38	19.8	S	K7	US-A
74	RX J1600.7-2343	16:00:44.6	-23:43:12	< 18.9	S	M2	US-A
75	RX J1601.1-2113	16:01:08.1	-21:13:19	22.2	S	M0	US-A
76	RX J1601.3-2652	16:01:18.4	-26:52:20	47.7	S	G0	US-A
77	RX J1601.4-2240[2]	16:01:25.6	-22:40:40	35.9	S	K1	US-A
78	RX J1601.7-2049	16:01:46.5	-20:49:46	26.9	S	M0	US-A
79	RX J1601.8-2445	16:01:51.5	-24:45:25	206.8	S/P	K7	US-A
80	RX J1601.9-2008	16:01:58.2	-20:08:12	78.9	S	G5	US-A
81	RX J1602.0-2221	16:02:00.4	-22:21:24	22.8	S	M1	US-A
82	RX J1602.1-2241[2]	16:02:10.5	-22:41:28	36.7	S	K4	US-A
83	RX J1602.8-2401B	16:02:51.3	-24:01:57	< 6.8	S	K4	US-A
84	RX J1602.8-2401A	16:02:52.4	-24:02:22	< 6.8	S	K0	US-A
85	RX J1602.9-2022	16:02:54.0	-20:22:48	58.8	S	K7	US-A
86	RX J1603.6-2245	16:03:35.5	-22:45:56	113.1	S	G9	US-A
87	RX J1603.9-2031B	16:03:55.0	-20:31:39	23.2	S	M0	US-A
88	RX J1603.9-2031A	16:03:57.7	-20:31:06	23.2	S	K5	US-A
89	RX J1604.3-2130B	16:04:20.9	-21:30:42	14.7	S	M2	US-A
90	RX J1604.3-2130A	16:04:21.7	-21:30:29	14.7	S	K2	US-A
91	RX J1604.7-1930[2]	16:04:47.7	-19:30:23	21.9	S	K3	US-A
92	RX J1605.6-2152	16:05:38.9	-21:52:32	20.2	S	M1	US-A
93	RX J1605.7-2004[2]	16:05:42.7	-20:04:15	11.2	S	M1	US-A
94	RX J1606.2-2036	16:06:12.6	-20:36:47	30.9	S	K5	US-A
95	RX J1606.3-1928[2]	16:06:22.0	-19:28:44	16.0	S	M0	US-A
96	RX J1606.6-2108	16:06:37.4	-21:08:41	9.6	S	M1	US-A
97	RX J1607.0-2043	16:07:03.1	-20:43:20	27.5	S	M1	US-A
98	RX J1607.0-2036	16:07:03.6	-20:36:26	38.8	S	M0	US-A
99	RX J1607.0-1911	16:07:03.9	-19:11:33	62.4	S	M1	US-A

[1]: In cases where more than one star was found within the error box of one X-ray source, we divided the X-ray counts equally among them
[2]: These stars were already discovered by Walter et al. (1994).

data reduction was publicly available at the time this survey was started. Therefore we used the `speckle` program written by one of us (R.K.). In this program, the modulus of the complex visibility (i. e. the Fourier transform of the object brightness distribution) is determined from power spectrum analysis, the phase is computed using the Knox-Thompson algorithm (Knox & Thompson 1974), and from the bispectrum (Lohmann et al. 1983). For a more detailed description see the appendix. Fig. 2 shows examples of the reconstructed images in Fourier space as well as images reconstructed by back transformation.

Analytically, the modulus of the complex visibility of a binary with the 2-dimensional separation vector $\boldsymbol{s}$ and a flux ratio of R is

$$|\tilde{O}(\boldsymbol{u})| = \sqrt{\frac{1 + 2R\cos(2\pi\boldsymbol{us})) + R^2}{1 + 2R + R^2}} \ .$$

This expression has been normalized to be 1 at spatial frequency $\boldsymbol{u} = 0$. The cosine term leads to the characteristic fringe pattern that can be seen in the examples of Fig. 2. The phase φ of the complex visibility can be written as

$$\tan\varphi = \frac{2\sin(\pi\boldsymbol{us})\cdot\cos(\pi\boldsymbol{us}\frac{1-R}{1+R}) - (1+R)\cdot\sin(2\pi\frac{\boldsymbol{us}}{1+R})}{2\sin(\pi\boldsymbol{us})\cdot\sin(\pi\boldsymbol{us}\frac{1-R}{1+R}) + (1+R)\cdot\cos(2\pi\frac{\boldsymbol{us}}{1+R})}.$$

These expressions cannot be solved to compute the binary parameters directly from the data. Therefore, we use a multidimensional least-squares fit using the `amoeba` algorithm (Press et al. 1994). Our program tries to minimize the difference between modulus and phase computed from a model binary and the observational data by varying the separation, position angle, and brightness ratio of the model. Fits to different subsets of the data yield an estimate for the standard deviation of the binary parameters.

If the object appears unresolved, we compute the maximum brightness ratio of a companion that could be hidden in the noise of the data. The principle is to determine how far the data deviate from the nominal result for a point source (modulus $= 1$, phase $= 0$). We then compute the brightness ratio of a companion that would result in this amount of deviation. This is repeated for position angles varying from $0°$ to $360°$ in steps of $10°$, and the maximum is used as upper limit for the brightness ratio of an undetected companion. See Leinert et al. (1997) for a more detailed description of this procedure.

Since it is very easy to distinguish the fringe pattern of a binary from noise in the data, there are no ambiguous cases in this survey where it is difficult to decide if a given star has a companion or not.

In order to find binaries that are separated by more than $3''$, we obtained additional infrared images with the ESO/MPIA 2.2 m telescope on La Silla in March 1996 using the IRAC2b camera.

4. Results

4.1. Uncorrected data

Tables 2 and 3 list all the binary and multiple stars we find in our sample. The Tables 4 and 5 list all stars where we did not find a companion and give limits for the brightness of an undetected companion. Fig. 3 shows these results as a plot of flux ratio and magnitude difference vs. binary separation. In total, among the 118 systems of the sample we find 41 binary and 6 triple stars.

The diffraction limit of the 3.5 m telescope at K for binary stars is $0.13''$. The modulus of the complex visibility of a binary is a cosine-shaped function. If the separation of the binary is equal to the diffraction limit, exactly one period of the modulus of the visibility fits within the radius where the optical transfer function of the telescope is not zero. Under good circumstances, it is possible to discover binaries with even smaller separations, down to about half the diffraction limit (Tables 2 and 3 show that we actually do find some). However, in these cases we can detect only the first minimum, but not the second maximum of the modulus of the visibility. Therefore, we cannot distinguish with certainty a close binary star below the diffraction limit from an elongated structure. Furthermore, we can't be sure that we find *all* companions at separations less than the diffraction limit. For these reasons, we limit ourselves to companions in the separation range between $0.13''$ and $6''$. The upper limit was chosen so that contamination with background stars has little effect (see Sect. 4.3 for a detailed discussion of this problem).

Five binaries and one component of a triple system have separations smaller than $0.13''$. The five binaries are treated as unresolved stars in our survey, while the triple system has to be degraded to a binary. This yields 37 binaries and 5 triples, i. e. 47 companion stars. For ease of comparison we mention that these uncorrected data correspond to a fractional multiplicity (number of multiples divided by total number of systems) of 0.36 ± 0.05 or to a number of 0.40 ± 0.06 companions per primary. The merit of this uncorrected result is that it has the lowest statistical uncertainty.

4.2. The restricted sample

In order to homogenise the sample, we apply two criteria, one related to the quality of our measurements and one to the measured X-ray flux.

First, Fig. 3 shows not only the stars where we find companions, but also the sensitivity of our survey, i. e. the maximum brightness ratio of a possible undetected companion as a function of the separation. This sensitivity depends on factors like the atmospheric conditions at the time of the observations and the brightness of the target star. To avoid introducing a bias caused by observations with poor signal-to-noise ratio, we define a restricted sample consisting of stars where our observations would allow us to detect any companion at a separation between $0.13''$ and $6''$ and with a magnitude difference to the primary of less than 2.5^{mag}. This corresponds to a brightness ratio of 0.1.

After inspection of the sensitivity curves of the individual observations we decided to exclude the 7 stars which are marked in Tables 4 and 5 by a '†'.

Our observations of a few of the remaining stars are not sufficient to exclude reliably companions with a brightness ratio near 0.1 at small separations (see Tables 4 and 5). However, based on the number of companions actually found, we expect
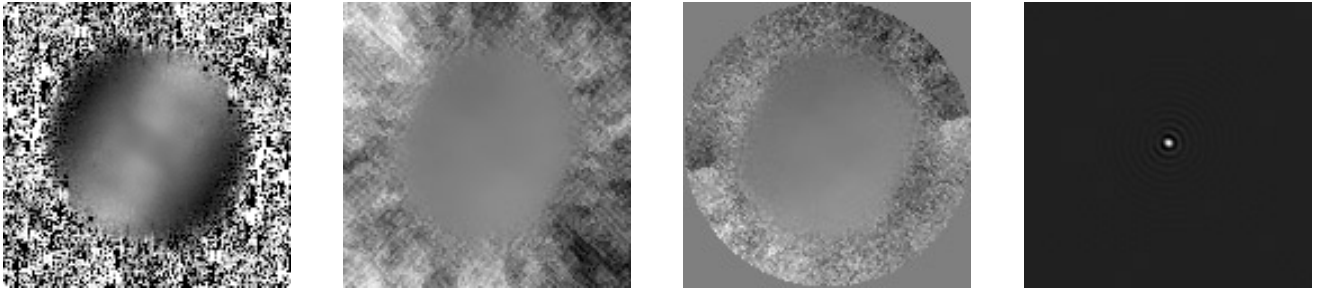
RX J1602.9-2022
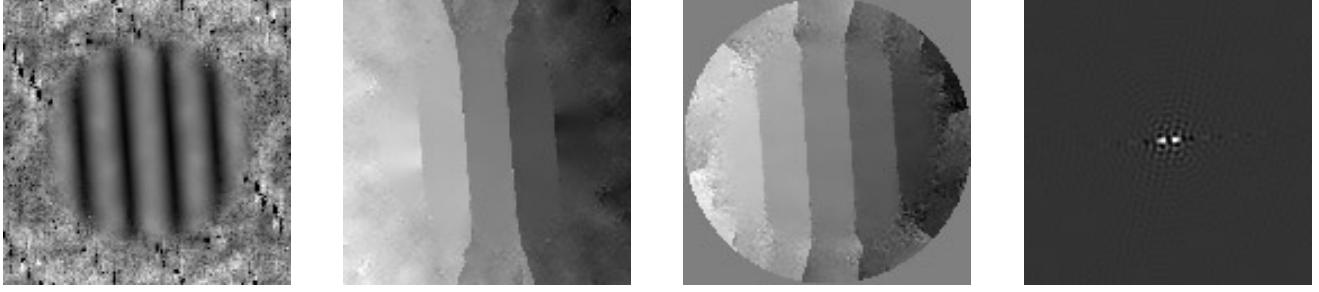
RX J1544.0-3311
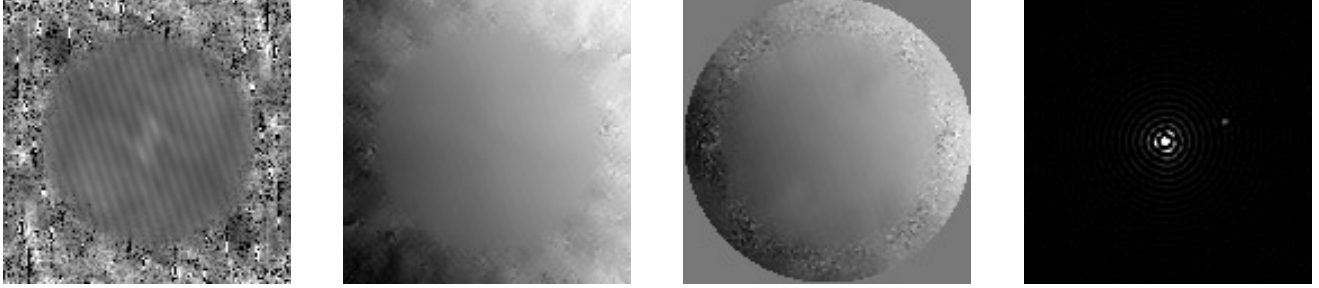
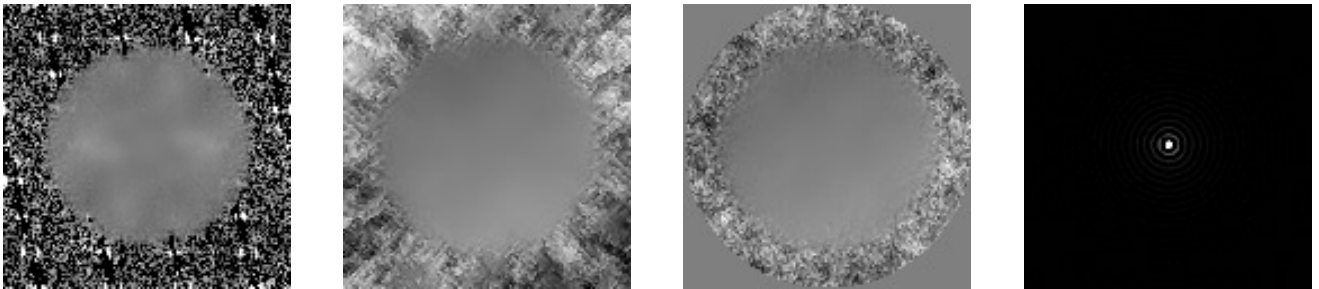
RX J1604.3-2130B

RX J1539.0-2956

Fig. 2. Examples for our speckle-interferometric data. From left to right, each row shows the modulus of the complex visibility, the phase computed using the Knox-Thompson algorithm, the phase computed from the bispectrum, and the image we obtain by Fourier transforming the complex visibility back into normal space. Since the bispectrum method requires a lot of computing time, we calculate the phase only within a circular area. The first row contains the results for a well-separated binary. The modulus shows the fringe pattern characteristic for a binary, while the phase is nearly a step function, where the jumps are at points corresponding to minima of the modulus. The second row shows images of a binary with a very faint companion (flux ratio 0.07). In fact, this is the faintest companion that was found with speckle observations in this survey, all the fainter companions were found by direct imaging. Even in this case the fringe pattern is clearly visible. The third row shows a marginaly resolved star (separation $0.08''$). In our data, the object is only elongated, but not resolved into two components. Therefore, we do not count stars like this in our binary statistic. The bottom row shows an unresolved star. In this case, the modulus and phase of the visibility are more or less constant. In all cases, the signal of the star in fourier space vanishes beyond a certain distance from the center. This is caused by the optical transfer function of the telescope, which is zero for frequencies higher than a maximum frequency that corresponds to the diffraction limit of the telescope

Table 2. Binary and triple WTTS among the stars discovered by W94. The first column gives the working numbers as in Table 3 of W94; the second gives the official designation; the third column specifies to which pair of a higher-order multiple system the following parameters apply; the fourth column gives the total system brightness in K. The following columns contain the date of the observation and the position and brightness of the companion relative to the primary (i. e. the star brighter in K). For a description of the way the errors were determined see text. If a companion was observed more than once, the different observations are listed in separate rows

No.	Designation		m_K [mag]	Date of Observation	Separation ["]	Position Angle [°]	Brightness Ratio at K
005	NTTS 155203-2338[1]		7.06	1. May 94	0.758 ± 0.007	234.2 ± 1.6	0.160 ± 0.008
				12. July 95	0.766 ± 0.003	232.0 ± 0.1	0.163 ± 0.006
008A	NTTS 155219-2314		9.35	3. May 94	1.485 ± 0.003	102.9 ± 0.3	0.366 ± 0.026
013	NTTS 155331-2340		8.76	3. May 94	0.092 ± 0.006	169.8 ± 5.0	0.567 ± 0.048
016	NTTS 155427-2346		8.96	3. May 94	1.324 ± 0.003	226.0 ± 0.4	$0.56 \ \pm 0.11$
020	NTTS 155808-2219		8.80	2. May 94	0.193 ± 0.005	313.7 ± 1.2	$0.57 \ \pm 0.1$
023	NTTS 155913-2233[1]		8.08	1. May 94	0.304 ± 0.003	346.0 ± 0.3	0.566 ± 0.016
				3. May 94	0.297 ± 0.003	345.2 ± 0.5	0.547 ± 0.01
029	NTTS 160248-1956[1]		9.12	2. May 94	0.643 ± 0.003	352.6 ± 0.4	0.595 ± 0.027
031	NTTS 160328-1921[1]		8.66	2. May 94	0.578 ± 0.003	148.2 ± 0.3	0.555 ± 0.007
042B	NTTS 160728-1856	AB	6.59	27. Feb. 96	4.604 ± 0.011	96.5 ± 0.1	0.117 ± 0.001
		AC		27. Feb. 96	4.201 ± 0.022	59.9 ± 0.1	0.016 ± 0.001
042A	NTTS 160735-1857		8.73	2. May 94	0.299 ± 0.003	84.1 ± 0.3	0.679 ± 0.035
048	NTTS 160905-1859		8.08	12. July 95	3.429 ± 0.009	12.3 ± 0.2	0.208 ± 0.007
052	NTTS 160946-1851		7.49	2. May 94	0.203 ± 0.006	161.9 ± 0.4	0.228 ± 0.027

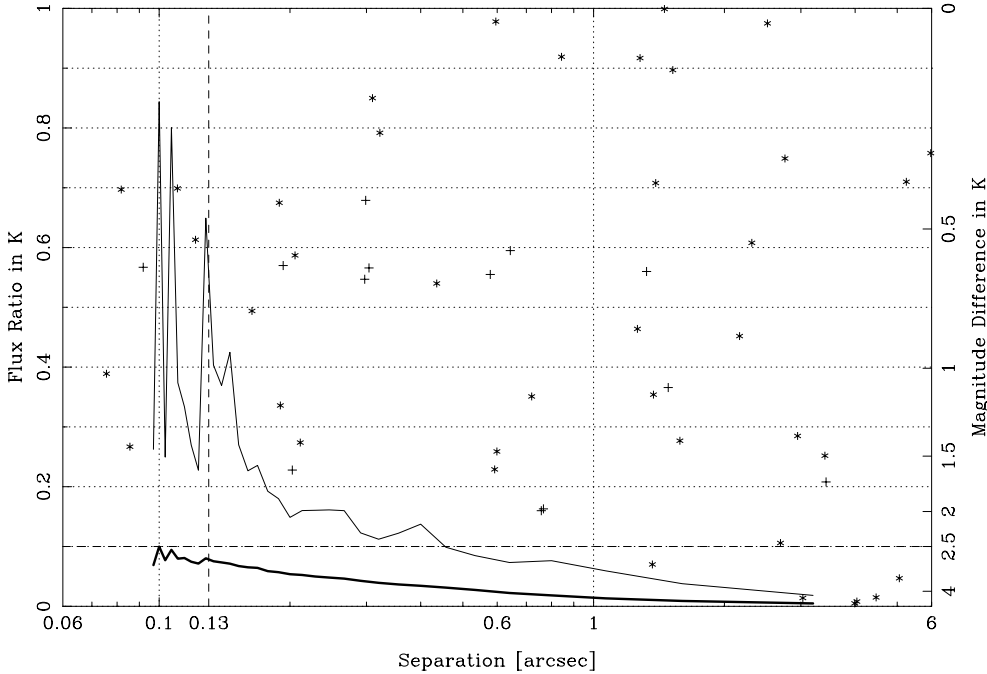[1]: These stars have also been discovered by Kunkel (1999).

Fig. 3. The results of our multiplicity survey in a plot of flux ratio or magnitude difference vs. binary star separation. The thick line shows the average, the thin line the worst sensitivity for undetected companions. The dashed vertical line at $0.13''$ shows the diffraction limit for a $3.5\,\mathrm{m}$ telescope at K. This is the limit for unambiguous identification of binary stars. The dashed horizontal line shows the completeness limit in flux ratio for the whole survey. Each observation of a companion is marked individually, i. e. some companions occur more than once in this diagram. Stars discovered by W94 are marked by crosses $(+)$, those discovered by K99 by asterisks $(*)$

about 0.25 additional companions above a brightness ratio of 0.1 at separations $< 0.5''$. Therefore, we are confident we have found all companions in the restricted sample of 111 stars within the parameter range defined above.

Second, there are several cases of uncertain X-ray detection, where only upper limits could be given for a possible X-ray flux, but where nevertheless young stars have been found in the surrounding error box. These additional 7 stars were also not included in the restricted sample; they are marked by an 'X' in Tables 3 and 5.

Therefore, the restricted sample contains only stars with valid X-ray detection, and where all companions with a magnitude difference of less than 2.5^{mag} have been detected. It consists of 104 systems, of which 36 are binaries and 5 are triples.

Table 3. Binary and triple stars among the TTS discovered by K99. The first column gives the running number as in Table 1; the second gives the official designation; the third column specifies to which pair of a higher-order multiple system the following parameters apply; the fourth column gives the total system brightness in K. The following columns contain the date of the observation and the position and brightness of the companion relative to the primary (i. e. the star brighter in K). For a description of the way the errors were determined see text. If a companion was observed more than once, the different observations are listed in separate rows

No.	Designation		m_K [mag]	Date of Observation	Separation ["]	Position Angle [°]	Brightness Ratio at K
2	RX J1524.2-3030B			1. May 94	3.408 ± 0.003	303.2 ± 0.3	0.252 ± 0.004
4	RX J1528.7-3117		6.82	30. Apr. 94	2.168 ± 0.005	185.2 ± 0.5	0.452 ± 0.004
5	RX J1529.4-2850A			10. July 95	1.580 ± 0.003	351.0 ± 0.1	0.277 ± 0.038
7	RX J1530.4-3218		6.92	30. Apr. 94	1.522 ± 0.003	27.6 ± 0.3	0.897 ± 0.01
10	RX J1531.5-3021	A-B	8.83	11. July 95	0.211 ± 0.006	28.6 ± 0.4	0.274 ± 0.015
		AB-C		11. July 95	1.261 ± 0.003	15.4 ± 0.1	0.464 ± 0.013
13	RX J1535.8-2958		9.38	1. May 94	0.844 ± 0.003	254.4 ± 0.3	0.919 ± 0.072
14	RX J1536.5-3246		9.61	30. Apr. 94	2.313 ± 0.003	317.0 ± 0.3	0.608 ± 0.006
15/16	RX J1537.0-3136	Aa	7.13	30. Apr. 94	1.390 ± 0.003	134.5 ± 0.3	0.708 ± 0.02
		Aa-B		30. Apr. 94	5.247 ± 0.009	107.2 ± 0.3	0.710 ± 0.019
19	RX J1538.9-3116	AB	9.55	10. July 95	0.720 ± 0.003	239.5 ± 0.3	0.351 ± 0.015
		AB-C		3. Mar. 96	4.470 ± 0.019	192.3 ± 0.3	0.015 ± 0.006
25	RX J1539.5-2953		10.39	11. July 95	0.190 ± 0.011	249.1 ± 2.8	0.336 ± 0.033
27/28	RX J1540.7-3121	A-B	10.41	10. July 95	5.973 ± 0.003	75.2 ± 0.1	0.758 ± 0.009
32	RX J1543.8-3306		9.44	3. Mar. 96	2.758 ± 0.011	186.2 ± 0.2	0.749 ± 0.02
33	RX J1544.0-3311	AB	8.34	30. Apr. 94	1.366 ± 0.008	199.5 ± 0.3	0.070 ± 0.003
		AB-C		4. Mar. 96	3.992 ± 0.008	75.6 ± 0.1	0.005 ± 0.001
35	RX J1545.2-3417		6.56	30. Apr. 94	2.693 ± 0.004	299.9 ± 0.3	0.106 ± 0.001
40	RX J1546.1-2804		7.38	1. May 94	0.110 ± 0.003	41.2 ± 0.5	0.699 ± 0.012
45	RX J1549.3-2600		7.96	1. May 94	0.164 ± 0.003	320.3 ± 0.4	0.494 ± 0.023
49	RX J1551.4-3131		9.06	30. Apr. 94	0.435 ± 0.003	181.9 ± 0.4	0.540 ± 0.017
51/52	RX J1552.5-3224		9.84	30. Apr. 94	2.514 ± 0.003	263.7 ± 0.3	0.975 ± 0.015
54	RX J1554.0-2920		8.69	1. May 94	1.373 ± 0.003	77.8 ± 0.3	0.354 ± 0.023
55	RX J1554.9-2347[1]		7.05	12. July 95	0.766 ± 0.003	232.0 ± 0.1	0.163 ± 0.006
56	RX J1555.1-2521		8.50	10. July 95	0.322 ± 0.003	100.8 ± 0.1	0.792 ± 0.018
58	RX J1555.6-3159		8.66	30. Apr. 94	3.032 ± 0.004	305.1 ± 0.3	0.014 ± 0.001
60	RX J1557.3-2529		8.83	10. July 95	0.596 ± 0.005	142.5 ± 0.2	0.978 ± 0.021
62	RX J1558.1-2405B		10.93	22. Aug. 96	0.592 ± 0.003	85.1 ± 0.1	0.229 ± 0.003
66	RX J1559.2-2606		9.04	1. May 94	2.949 ± 0.004	331.4 ± 0.3	0.285 ± 0.013
68	RX J1559.8-2556		9.25	1. May 94	5.058 ± 0.016	92.7 ± 0.3	0.047 ± 0.006
71	RX J1600.5-2027		8.81	2. May 94	0.189 ± 0.004	171.7 ± 0.5	0.675 ± 0.037
74	RX J1600.7-2343[X]		9.66	12. July 95	1.456 ± 0.003	209.7 ± 0.1	0.999 ± 0.093
76	RX J1601.3-2652		7.54	1. May 94	0.086 ± 0.003	354.4 ± 1.7	0.267 ± 0.033
78	RX J1601.7-2049		8.61	2. May 94	0.205 ± 0.003	324.7 ± 0.9	0.587 ± 0.026
79	RX J1601.8-2445		8.51	10. July 95	0.076 ± 0.005	289.6 ± 10.0	0.389 ± 0.064
82	RX J1602.1-2241[1]		8.03	1. May 94	0.304 ± 0.003	346.0 ± 0.3	0.566 ± 0.016
85	RX J1602.9-2022		8.14	2. May 94	0.310 ± 0.008	5.3 ± 0.3	0.850 ± 0.066
87	RX J1603.9-2031B	AB	8.61	2. May 94	0.121 ± 0.003	140.9 ± 0.6	0.613 ± 0.034
		AB-C		4. Mar. 96	4.037 ± 0.011	81.6 ± 0.1	0.008 ± 0.001
89	RX J1604.3-2130B		9.24	1. May 94	0.082 ± 0.003	327.4 ± 0.8	0.70 ± 0.126
93	RX J1605.7-2004[1]		9.19	2. May 94	0.643 ± 0.003	352.6 ± 0.4	0.595 ± 0.027
95	RX J1606.3-1928[1]		8.53	2. May 94	0.578 ± 0.003	148.2 ± 0.3	0.555 ± 0.007
96	RX J1606.6-2108		9.04	1. May 94	1.279 ± 0.003	33.9 ± 0.3	0.917 ± 0.001
99	RX J1607.0-1911		8.92	2. May 94	0.599 ± 0.003	87.6 ± 0.3	0.259 ± 0.002

[1]: These stars were already discovered by Walter et al. (1994).
[X]: Only an upper limit for the X-ray flux of this star is known.

Table 4. Unresolved stars among the TTS of W94 and limits for undetected companions.

No.	Designation	m_K [mag]	Date of Observation	Maximum Flux Ratio		Minimal Δm_K [mag]	
				at $0.13''$	at $0.5''$	at $0.13''$	at $0.5''$
008B	NTTS 155220-2313	9.71	3. May 94	0.16	0.07	1.99	2.89
014	NTTS 155357-2321[†]	10.31	3. May 94	1.00	1.00	0.00	0.00
015	NTTS 155421-2330	8.85	3. May 94	0.40	0.12	0.99	2.30
017	NTTS 155436-2313	8.93	2. May 94	0.06	0.03	3.05	3.81
019	NTTS 155703-2212	8.62	2. May 94	0.09	0.05	2.61	3.25
021	NTTS 155828-2232[1]	8.49	12. July 95	0.06	0.03	3.05	3.81
022	NTTS 155910-2247	9.52	3. May 94	0.08	0.04	2.74	3.49
027	NTTS 160153-1922[1]	8.06	2. May 94	0.05	0.04	3.25	3.49
028	NTTS 160233-1931	9.61	2. May 94	0.06	0.03	3.05	3.81
032	NTTS 160345-1953	10.07	2. May 94	0.11	0.08	2.40	2.74
044	NTTS 160814-1857	7.68	2. May 94	0.09	0.03	2.61	3.81
045	NTTS 160827-1813	8.53	12. July 95	0.05	0.04	3.25	3.49
046	NTTS 160836-1843	9.61	2. May 94	0.05	0.03	3.25	3.81
051	NTTS 160927-1901	9.67	2. May 94	0.04	0.04	3.49	3.49
060	NTTS 161431-2256	7.93	3. May 94	0.14	0.12	2.13	2.30
214	NTTS 162649-2145	7.78	3. May 94	0.06	0.01	3.05	5.00

[1]: These stars have also been discovered by Kunkel (1999).

[†]: We exclude these stars from the restricted sample because of their poor signal-to-noise ratio.
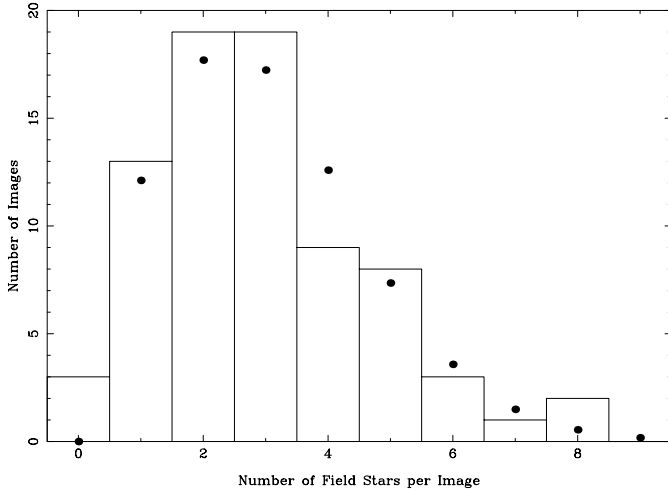
Fig. 4. Distribution of the number of field stars in 77 images. The histogram shows the number of background stars we count in our images; the dots denote a Poisson distribution with the same average star density

4.3. Confusion with background stars

From our data, we have no possibility to decide if a given binary is indeed a physically bound pair or a chance association with a field star. We expect a certain number of wide binaries to appear as binary only due to chance projections. To estimate this number, we use the infrared images obtained at the ESO/MPIA 2.2 m telescope and count the field stars in 77 of these images. We exclude a circular area with a radius of $15''$ around the T Tauri star in each image to avoid counting physically bound companions. This leaves $4400\,\mathrm{arcsec}^2$ per field, giving a total area of $93\,\mathrm{arcmin}^2$. The fact that these are the same images we use to search for companions ensures that we have the same magnitude limit for field stars as for companion stars.

Fig. 4 shows the distribution of field stars we obtain using this procedure. The measured distribution can be approximated by a Poisson distribution with a mean of 2.92. The corresponding field star density is $(6.64 \pm 0.45) \cdot 10^{-4}$ stars per arcsec^2.

With this result, we can compute the expected number of field stars within a projected distance of $6''$ to one of the 104 T Tauri stars of our restricted sample:

$$(6.64 \pm 0.45) \cdot 10^{-4} \cdot \pi \cdot 6^2 \cdot 104 = 7.8 \pm 0.5 \,.$$

The probability for *one* object to be associated with a field star is $7.8/104 = 7.5\,\%$.

We obtain an estimate for the number of physically bound companions by subtracting the number of chance associations from the total number of companions, i. e. $46 - 7.8 \approx 38$ to 39 companion stars. When we correct the number of binaries and triples, we must take into account that a binary caused by a chance projection is in fact a single star, so the number of "false" binaries depends on the true number of single stars. This way, we arrive at the result that 5 binaries and 2.5 triples are caused by chance associations. The corrected numbers of physically bound systems are 33 binaries and 3 triples, which yields a total of 39 companions.

4.4. Bias induced through X-ray selection

It was pointed out by Brandner et al. (1996) that the flux limit of X-ray selected samples induces a detection bias in favor of binary and multiple stars. Since binaries are on average brighter X-ray sources than single stars, there is a small number of binaries with an X-ray flux of the individual components below,

Table 5. Unresolved stars among the TTS of K99 and limits for undetected companions.

No.	Designation	m_{K} [mag]	Date of Observation	Maximum Flux Ratio		Minimal Δm_{K} [mag]	
				at $0.13''$	at $0.5''$	at $0.13''$	at $0.5''$
1	RX J1524.2-3030A	8.96	1. May 94	0.06	0.02	3.05	4.25
3	RX J1528.0-2600	8.58	1. May 94	0.09	0.06	2.61	3.05
6	RX J1529.4-2850B[†]		10. July 95	1.0	0.39	0.00	1.02
8	RX J1530.8-3021	8.68	1. May 94	0.06	0.02	3.05	4.25
9	RX J1531.3-3329	8.76	30. Apr. 94	0.05	0.03	3.25	3.81
11	RX J1534.3-3300	8.82	9. July 95	0.02	0.02	4.25	4.25
12	RX J1535.2-2828		10. July 95	0.04	0.03	3.49	3.81
17	RX J1537.8-3045	8.58	1. May 94	0.06	0.06	3.05	3.05
18	RX J1538.2-3229		9. July 95	0.20	0.10	1.75	2.50
20	RX J1539.0-2956		1. May 94	0.07	0.04	2.89	3.49
21	RX J1539.4-2958[†]		11. July 95	0.37	0.22	1.08	1.64
22	RX J1539.4-3446A	7.43	30. Apr. 94	0.04	0.03	3.49	3.81
23	RX J1539.4-3446B	7.95	1. May 94	0.11	0.05	2.40	3.25
24	RX J1539.4-3446C	8.87	1. May 94	0.14	0.07	2.13	2.89
26	RX J1540.2-3018[†]	11.85	11. July 95	0.66	0.34	0.45	1.17
29	RX J1540.9-3024	9.36	11. July 95	0.20	0.12	1.75	2.30
30	RX J1541.9-3019[†]	11.18	11. July 95	0.34	0.27	1.17	1.42
31	RX J1543.4-2925	8.53	1. May 94	0.05	0.03	3.25	3.81
34	RX J1544.2-3117	10.24	10. July 95	0.20	0.06	1.75	3.05
36	RX J1545.5-3249[X]	9.82	9. July 95	0.10	0.04	2.50	3.49
37	RX J1545.6-3208[X]	7.49	30. Apr. 94	0.03	0.02	3.81	4.25
38	RX J1545.8-3020	6.56	30. Apr. 94	0.10	0.07	2.50	2.89
39	RX J1546.0-2920[X][†]	9.48	11. July 95	1.0	1.0	0.00	0.00
41	RX J1546.7-3210	10.30	22. Aug. 96	0.14	0.10	2.13	2.50
42	RX J1548.0-2908	8.62	1. May 94	0.05	0.05	3.25	3.25
43	RX J1548.9-3045	10.30	10. July 95	0.12	0.07	2.30	2.89
44	RX J1549.0-3102	8.63	30. Apr. 94	0.10	0.06	2.50	3.05
46	RX J1550.0-2312[X]	12.48	5. May 98	0.10	0.09	2.50	2.61
47	RX J1550.9-2534	7.94	10. July 95	0.17	0.04	1.92	3.49
48	RX J1551.1-2402[†]	9.73	11. July 95	0.40	0.18	0.99	1.86

[1]: These stars were already discovered by Walter et al. (1994).
[X]: Only upper limits for the X-ray flux of these stars are known.
[†]: We exclude these stars from the restricted sample because of their poor signal-to-noise ratio.

but combined flux above the cut-off. These systems cause an overestimate of the binary frequency.

Since we are detecting only companions within a limited range of separations, the unresolved stars in our sample will contain a fraction of "hidden" binaries, among which there will be a number of systems which would not have entered the sample were it not for the additional X-ray flux of the companion. These systems cause an underestimate of the binary frequency.

One might argue that the X-ray selected sample is approximately complete since Preibisch et al. (1998) didn't find any PMS stars among a list of 100 stars that were not detected as X-ray sources, but have proper motions indicating membership to the Upper Scorpius association. However, the same authors estimate a completeness of only $80 - 90\,\%$. Furthermore, it would be a rather lucky coincidence if the sensitivity limit of the RASS would be identical to the cut-off of the X-ray luminosity function. For the bias discussed here, the number of stars with luminosities in the rather small interval L_{limit} to $L_{\mathrm{limit}}/2$ is impor-

tant. Therefore, we have to go into a more detailed discussion of these bias effects.

To do so, we use the X-ray counts that led to the detection of the star and check which binaries could have been detected only because of this bias. In the worst case, all binaries would consist of two components with equal X-ray fluxes. Then, all binaries with a number of X-ray counts N_x between N_{limit} and $2N_{\mathrm{limit}}$ would have to be excluded from the sample to remove the bias. However, we expect only a negligible fraction of binaries to consist of two equally bright components, and we would over-correct the bias if we discarded all binaries with $N_x < 2N_{\mathrm{limit}}$.

To obtain an estimate for the number of binaries with *both* components below N_{limit}, we apply the method described in Köhler & Leinert (1998). We use $\log(N_{\mathrm{limit}})+0.2$ as borderline for binaries and $\log(N_{\mathrm{limit}}) + 0.3$ as borderline for triples and treat all systems fainter than this as discovered because of the detection bias.

Table 5. (continued)

No.	Designation	m_K [mag]	Date of Observation	Maximum Flux Ratio		Minimal Δm_K [mag]	
				at $0.13''$	at $0.5''$	at $0.13''$	at $0.5''$
50	RX J1551.9-2621		10. July 95	0.03	0.02	3.81	4.25
53	RX J1552.5-2633	9.05	10. July 95	0.04	0.02	3.49	4.25
57	RX J1555.4-3338	9.30	9. July 95	0.05	0.02	3.25	4.25
59	RX J1555.8-2512	8.31	10. July 95	0.04	0.03	3.49	3.81
61	RX J1557.8-2305	8.98	11. July 95	0.21	0.02	1.69	4.25
63	RX J1558.1-2405A	8.94	12. July 95	0.17	0.05	1.92	3.25
64	RX J1558.2-2328	8.01	1. May 94	0.07	0.04	2.89	3.49
65	RX J1558.8-2512	9.31	10. July 95	0.08	0.05	2.74	3.25
67	RX J1559.6-3255	9.50	9. July 95	0.03	0.01	3.81	5.00
69	RX J1600.0-2509	8.79	10. July 95	0.06	0.01	3.05	5.00
70	RX J1600.2-2417[X]	11.03	12. July 95	0.06	0.05	3.05	3.25
72	RX J1600.6-2159	8.36	1. May 94	0.22	0.09	1.64	2.61
73	RX J1600.7-2127	8.90	1. May 94	0.04	0.03	3.49	3.81
75	RX J1601.1-2113	8.74	1. May 94	0.05	0.04	3.25	3.49
77	RX J1601.4-2240[1]	8.49	12. July 95	0.06	0.07	3.05	2.89
80	RX J1601.9-2008	7.68	2. May 94	0.07	0.03	2.89	3.81
81	RX J1602.0-2221	8.82	1. May 94	0.12	0.05	2.30	3.25
83	RX J1602.8-2401B[X]	8.73	22. Aug. 96	0.09	0.04	2.61	3.49
84	RX J1602.8-2401A[X]	7.52	10. July 95	0.06	0.04	3.05	3.49
86	RX J1603.6-2245	8.15	1. May 94	0.02	0.01	4.25	5.00
88	RX J1603.9-2031A	8.31	2. May 94	0.07	0.05	2.89	3.25
90	RX J1604.3-2130A	8.12	1. May 94	0.04	0.01	3.49	5.00
91	RX J1604.7-1930[1]	8.03	2. May 94	0.05	0.04	3.25	3.49
92	RX J1605.6-2152	9.53	9. July 95	0.04	0.02	3.49	4.25
94	RX J1606.2-2036	8.89	2. May 94	0.07	0.04	2.89	3.49
97	RX J1607.0-2043	9.58	9. July 95	0.04	0.02	3.49	4.25
98	RX J1607.0-2036	8.04	2. May 94	0.11	0.06	2.40	3.05

[1]: These stars were already discovered by Walter et al. (1994).
[X]: Only upper limits for the X-ray flux of these stars are known.
[†]: We exclude these stars from the restricted sample because of their poor signal-to-noise ratio.

Since the sensitivities of EINSTEIN and ROSAT are somewhat different, we have to use different values of N_{limit}. Therefore, we treat the stars discovered by W94 and K99 separately.

4.4.1. Stars discovered by Walter et al.

Fig. 5 shows the numbers of unresolved, binary and triple stars in the list of W94 vs. their X-ray counts. Although the numbers are quite small, there is a reasonably sharp decline at $10^{1.2}$ counts. The one star below this number (no. 214 = NTTS 162649-2145 with 10.4 counts) was found in a special reexaminination of the data (Walter, priv. comm.) and therefore has a number of counts smaller than the limit for the standard source detection. There is one binary (No. 020 = NTTS 155808-2219) below the corresponding limit for binaries of $10^{1.4}$ counts. We note that this star has not been rediscovered by K99. Its separation is $0.193\,\text{arcsec}$, so the probability for this star to be caused by chance alignment with a background star is negligible. Therefore, we conclude that the detection of this star was caused by the X-ray bias and remove it from our survey.

The count numbers of three unresolved stars are below the limit for binaries, these stars are suspect to be "hidden" binaries. They are considered in Sect. 4.4.3.
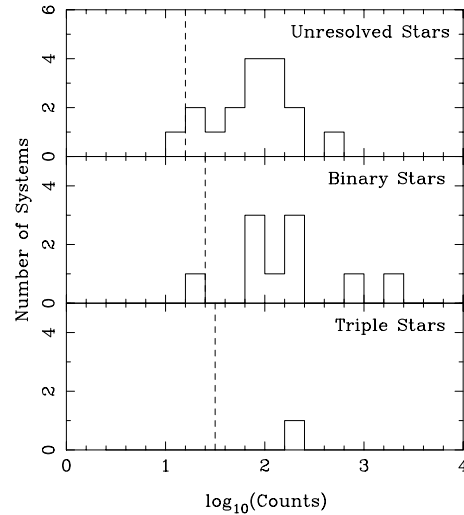

Fig. 5. Distribution of the number of X-ray counts of the stars discovered by EINSTEIN (W94), broken down into unresolved, binary, and triple systems. The vertical lines mark the limits chosen by us to obtain an unbiased sample: $N_{\text{limit}} = 10^{1.2}$ counts for unresolved stars, $\log(N_{\text{limit}}) + 0.2$ for binaries, and $\log(N_{\text{limit}}) + 0.3$ for triple stars. The unresolved star below N_{limit} was found in a special reexamination of the data (see text)
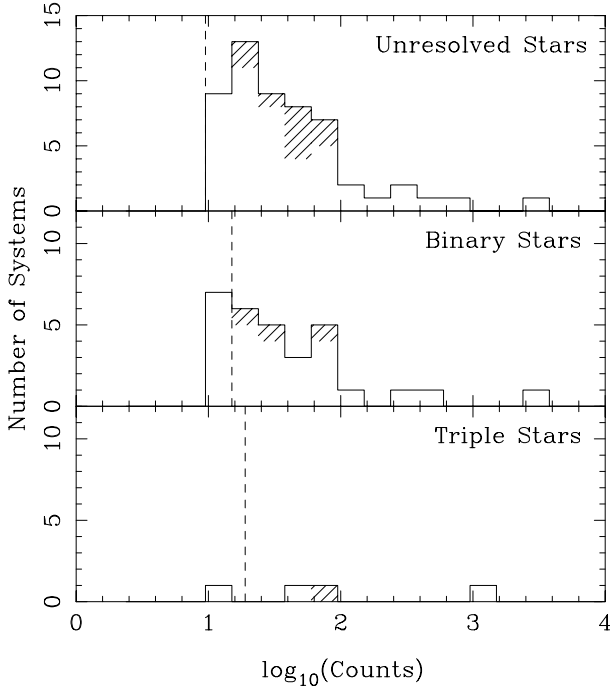
Fig. 6. Distribution of the number of X-ray counts of the stars discovered by ROSAT (K99), broken down into unresolved, binary, and triple systems. Stars discovered with pointed ROSAT observations are hatched, all the others have been found with the All-Sky Survey. The vertical lines mark the limits chosen by us to obtain an unbiased sample: the lowest measured value for unresolved stars (9.5 counts), $\log(N_{\mathrm{limit}}) + 0.2$ for binaries, and $\log(N_{\mathrm{limit}}) + 0.3$ for triple stars

4.4.2. Stars discovered by Kunkel

Fig. 6 shows the distributions of unresolved, binary and triple stars in the list of K99 over their X-ray counts. We use the lowest measured value of 9.5 counts as limit, since it is very close to the usually adopted value of 8. In Fig. 6, the binning has been adjusted accordingly. The figure shows that seven binaries and one triple are affected by the X-ray bias, and that nine unresolved stars might be "hidden" binaries affected by this bias.

One of these seven binaries (RXJ 1605.7-2004) was also detected by EINSTEIN. W94 report 211.87 counts, which is well above the detection limit. Therefore, we assume that this star is not affected by the X-ray bias, since it would have been detected by EINSTEIN even if it had only half the X-ray flux.

The situation is even further complicated because of the fact that some of the stars we expect to be affected by the X-ray bias could only appear to be binaries due to chance projections. In this case, the star would not be affected by the X-ray bias since the background star doesn't contribute to the X-ray flux. To investigate this problem, Fig. 7 shows a plot of X-ray counts vs. separation for the stars detected only by ROSAT. We expect 4.3 chance alignments among those stars in the separation range from $3''$ to $6''$ and we do find 8 companions, i.e. about half of those systems are due to chance projections. There are two companions potentially affected by the X-ray bias, so we expect one of them to be a single star with a background star nearby.
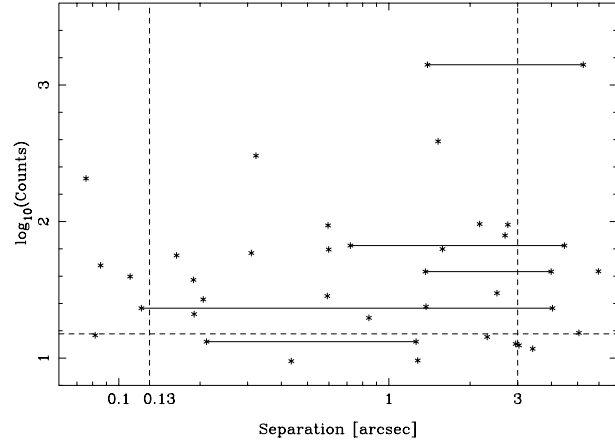
Fig. 7. X-ray counts vs. separation of the binary and triple stars discovered by ROSAT (K99). Each triple system is represented by two asterisks that are connected by a horizontal line

Only 1.6 among the 26 companions in the separation range from $0.13''$ to $3''$ are chance alignments. This yields an expected number of 0.3 chance projections among the 5 stars below the X-ray count limit, so probably all 5 stars are indeed affected by the X-ray bias.

In the end we find that the following systems are affected by X-ray bias: one triple system and five binaries among the stars discovered by K99 and one binary among the stars discovered by W94. This reduces our numbers to 27 binaries and 2 triples, in total 31 companions.

4.4.3. Unresolved stars affected by the X-ray bias

Three of the apparently single stars discovered by W94, and nine of the unresolved stars discovered by K99 might be "hidden" binaries affected by the X-ray bias.

If we assume a total fractional multiplicity of 0.84 (see Sect. 5.2), we get the result that 77 % of the stars unresolved by us are in fact multiple systems. Therefore, about 9 of the 12 candidates are indeed "hidden" binaries. Since the total fractional multiplicity is the end result after all the corrections, these numbers cannot be computed directly, but have to be found through an iterative process.

The corrected sample, free of chance projection and X-ray bias to the best of our knowledge, now consists of 88 primaries, of which 59 are single, 27 are binaries and 2 are triples. This corresponds to a fractional multiplicity of 0.33 ± 0.06 or to 0.35 ± 0.06 companions per primary. This is indeed close to the raw observed values of multiplicity, as one might expect for a sample of high intrinsic multiplicity (Brandner et al. 1996).

5. Discussion

5.1. Stars discovered with EINSTEIN compared to stars discovered with ROSAT

Since the surveys of W94 and K99 were conducted using different satellites (EINSTEIN and ROSAT), different instruments

(IPC and PSPC), and different methods (pointed observations and survey scans), resulting in different sensitivity limits, it is not a priori clear that both subsamples are representative for the same class of stars. A full discussion of the differences between the stars discovered by W94 and K99 is beyond the scope of this paper. Here, we want to concentrate on the binary properties of the two subsamples.

In total, the subsample of W94 has 41.6 ± 13.2 companions per 100 primaries, while the stars discovered by K99 have 35.7 ± 7.1. Within the statistical errors, the two numbers are the same. However, due to the small sample sizes, the errors are quite large.

The period distribution of both subsamples is shown in Fig. 8. Again, there is no difference between both distributions within the (large) statistical errors.

Therefore, we conclude that the binary properties of both subsamples are indistinguishable within the statistical errors. We continue to use the combined sample in order to keep the errors as small as possible.

5.2. Pre-main-sequence compared to main-sequence stars

To compare our pre-main-sequence stars to main-sequence stars, we use the results of the multiplicity survey of Duquennoy & Mayor (1991, DM91). There are other studies of main-sequence stars (e. g. Mayor et al. 1992; Fischer & Marcy 1992), but DM91 is not only the most comprehensive study, it also covers the range of spectral types most of our stars will have after they evolve to the main sequence (F and G).

To be able to do the comparison, we need to convert our measured angular separations into orbital periods. This is impossible for individual objects of our sample since the orbital parameters are not known. Instead, we follow the approach of Leinert et al. (1993) and Köhler & Leinert (1998), who rely on statistical arguments. First, we convert the angular separation into a linear separation. HIPPARCOS measurements yield a mean distance of $(145 \pm 2)\,\mathrm{pc}$ to Upper Scorpius and $(140 \pm 2)\,\mathrm{pc}$ to Upper Centaurus Lupus (de Zeeuw et al. 1999). We use a value of 145 pc for all stars of our sample since small changes in distance do not change our results. Furthermore, the extension of the star-forming region along the line of sight is probably much larger than 5 pc.

The second step is to convert the projected separation into a semi-major axis, taking into account the probability for a binary to be observed in a particular position in its orbit and the inclination of the orbital plane. These two effects lead to a combined reduction factor of 0.95 (see Leinert et al. 1993 for details). Finally, we use Kepler's third law with a system mass of $1\,\mathrm{M}_\odot$ to compute the orbital periods. With these numbers, the separation range $0.13''$ to $6''$ transforms into a range of periods from $10^{4.5}$ to 10^7 days.

After correction for chance projections and X-ray bias, our sample contains (35.2 ± 6.3) companions per 100 T Tauri stars. Within the range of periods covered by our survey, DM91 find (22.2 ± 3.7) companions per 100 main-sequence stars. In other words, we find (13.0 ± 7.3) additional companions per 100
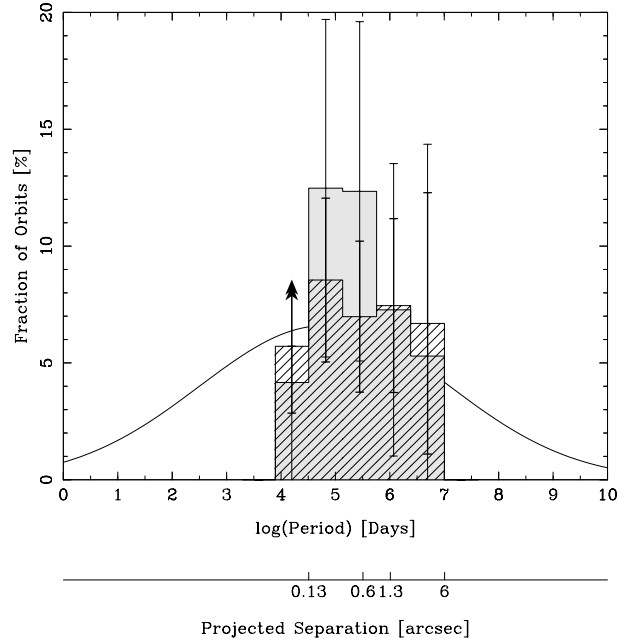

Fig. 8. Comparison of the binary period distributions of stars discovered with EINSTEIN (W94, shaded histogram and thin error bars) and stars discovered by ROSAT (K99, hatched histogram and thick error bars). The height of each bin shows the number of companion stars with orbital period in a given interval divided by the total number of systems. Therefore, triple systems are represented as two pairs. The number of companions with periods shorter than $10^{4.5}$ days is only a lower limit since it is difficult to resolve binaries with such a small separation. The curve shows the distribution of binaries among solar-type main-sequence stars (DM91)

T Tauri stars compared to solar-type main-sequence stars in the same range of orbital periods. The multiplicity of Pre-main-sequence stars in Upper Scorpius is enhanced by a factor of 1.59 ± 0.34. Fig. 9 shows the comparison of the period distributions.

According to DM91, their survey is complete for mass ratios larger than 0.1. We detected all binaries with brightness ratios in K larger than 0.1 to about 0.01, depending on the separation. For pre-main-sequence stars contracting along the Hayashi line, a proportionality or near-proportionality of K brightness and mass should be a good approximation (Simon et al. 1992, Zinnecker et al. 1992, Reipurth and Zinnecker 1993). However, as the stars evolve, the relation for the lower main sequence, $L \propto M^{1.6...2.5}$ (Henry & McCarthy 1993), should be approached. Therefore, we expect that our survey is not as complete as that of DM91. Furthermore, we do not add a correction for companions undetected because of detection biases as DM91 do. This means the enhancement factor of 1.59 is rather a lower limit.

Taking stars with *all* periods into account, DM91 find a fractional multiplicity, i. e. the number of multiple systems divided by the number of primaries, of 0.53 (see Leinert et al. 1993). If we assume that the shape of the period distribution is the same for main-sequence stars and the young stars in Upper Scorpius, we get the extrapolated multiplicity for companions with all periods of our sample by multiplying 0.53 with the enhancement
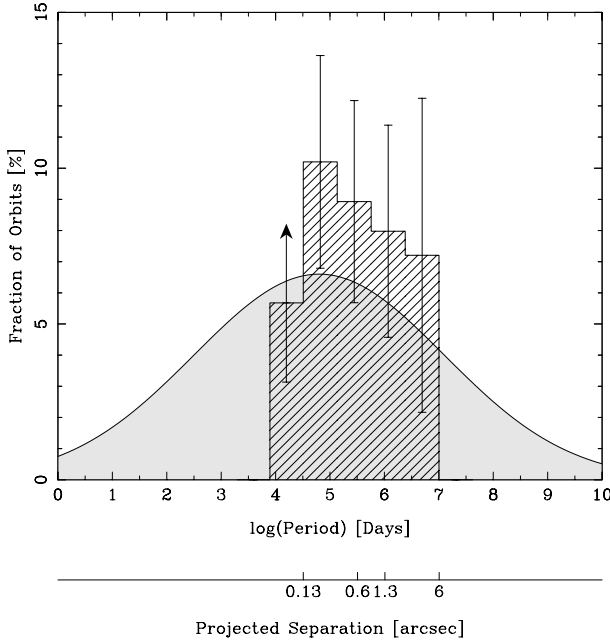
Fig. 9. Binary frequency as a function of orbital period and separation. The histogram shows the result of our survey; the shaded curve is the distribution of binaries among solar-type main-sequence stars (DM91). The number of companions with periods shorter than $10^{4.5}$ days is only a lower limit since it is difficult to resolve binaries with such a small separation. Therefore, we expect our survey to be incomplete in this regime

factor of 1.59. This yields about 0.84, i. e. most of the T Tauri stars in Upper Scorpius should be binary or multiple systems, if our assumptions for extrapolation are valid.

5.3. Scorpius-Centaurus compared to Taurus-Auriga

For Taurus-Auriga, we use the data of Leinert et al. (1993) and Köhler & Leinert (1998), who surveyed a sample of 174 T Tauri stars in the star-forming region Taurus-Auriga for companions in a similar way as we did in Upper Scorpius. Furthermore, we add the companion of Haro 6-37 that was discovered recently (Richichi et al. 1999). The parameters of this star are: separation 0.33", position angle 181°, flux ratio in K 0.1.

Within the period range from $10^{4.5}$ to 10^7 days, the Taurus-Auriga sample contains 68.0 ± 8.3 companion stars. This corresponds to 39.1 ± 4.7 companions per 100 T Tauri stars. Although this is slightly more than the (35.2 ± 6.3) companions per 100 T Tauri stars we find in Upper Scorpius, the difference is statistically not significant. Fig. 10 shows the period distribution of TTS in Taurus-Auriga and Scorpius-Centaurus, which are also the same within the errors. This suggests that the physical conditions for star formation in the Upper Scorpius OB association were closer to those encountered in a distributed T associations than to a cluster.

In contrast to the period distributions, we find a difference between the flux ratio distributions of binaries in the two star-forming regions (Fig. 11). The relative number of binaries with
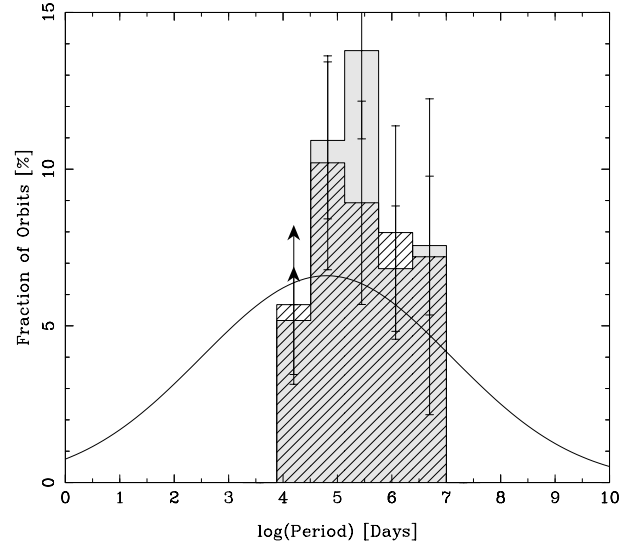

Fig. 10. Comparison of the period distributions of binaries in Taurus-Auriga (shaded histogram, adapted from Köhler & Leinert 1998) and in Scorpius Centaurus (hatched histogram, this work). The curve shows the distribution of binaries among solar-type main-sequence stars (DM91)

components of equal or nearly equal brightness is higher among stars in Taurus-Auriga than among stars in Scorpius-Centaurus. Since these binaries are easiest to detect, there is no reason to assume that our survey in Scorpius-Centaurus should have missed some of them. This is in agreement with the findings of Ghez et al. (1997), who also found a relatively high fraction of equal flux components in Taurus compared to southern star forming regions. However, a χ^2 test of our data did not yield a statistically significant difference between the two distributions.

5.4. Comparison of subgroups in Ophiuchus-Scorpius-Centaurus

Brandner et al. (1996) noted different binary frequencies among stars north of $\delta = -28°$ (subgroup "US-A") and stars south of this line (subgroup "US-B"). Our speckle observations revealed that this is caused by a difference in the distributions of binary separations: The peak of the distribution for stars in US-A is at 90 AU, while the peak for stars in US-B is at about 215 AU (Brandner & Köhler 1998).

The inclusion of binaries with separations in the range 3" to 6" further strengthens this result: the peak for stars in US-A is at about 50 AU, while the relatively large number of binaries with separations $> 3"$ in US-B shifts the peak of the distribution to about 350 AU (see Fig. 12). A χ^2 test gives only a probability of about 1 % that both samples were drawn from the same distribution.

Of course, the correction for chance projections with background stars has to be done very carefully. In creating Fig. 12, this was done for each bin individually, using the total number of systems in the corresponding subgroup and the area of the corresponding annulus on the sky. Our counts of field stars show
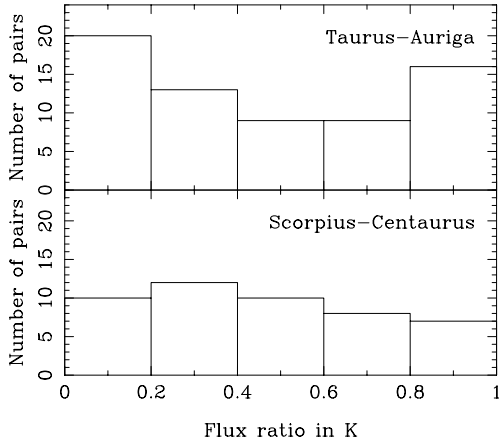
Fig. 11. Comparison of the flux-ratio distributions of binaries in Taurus-Auriga (Köhler & Leinert 1998) and in Scorpius Centaurus (this work)

Fig. 12. Comparison of binaries in different subgroups. The upper panel shows the period distribution of binaries located in the Ophiuchus star-forming region (Simon et al. 1995), the middle and lower panel show the results for stars in Upper Scorpius A and B, resp. (this work)

that the background star density is the same in US-A and US-B: 44 of the images mentioned in Sect. 4.3 are located in US-A and contain on average (2.75 ± 0.24) field stars, while 33 images lie in US-B and contain (3.15 ± 0.34) field stars.

Fig. 12 also shows results from Simon et al. (1995), who surveyed 35 targets in the Ophiuchus star-forming region by means of lunar occultations and direct imaging. The period distribution they obtain is remarkably similar to the distribution in US-A. A χ^2 test yields a propability of about 80 % that the Ophiuchus and US-A samples were drawn from the same distribution, while the probability is only 5 % for the Ophiuchus and the US-B samples. This is in agreement with the scenario presented by Preibisch & Zinnecker (1999): They propose that star formation in Upper Scorpius was triggered by a supernova in Upper Centaurus Lupus (UCL), while star formation in Ophiuchus was triggered by one in Upper Scorpius (US). If star formation was triggered in both regions, it is probably not too surprising that the binary period distributions are similar.

The division between US-A and US-B approximately matches the borderline between Upper Scorpius and Upper Centaurus Lupus (see Fig. 1). In fact, proper motion data of the stars in our sample show (Frink 1999 and priv. comm.) that all of the stars south of $\delta = -28°$ belong to UCL, while north of this line stars from US and stars from UCL can be found.

The star formation in Upper Scorpius is already finished and the remaining interstellar gas has been dispersed. We have no way to actually measure the physical conditions in the molecular cloud that gave birth to the young stars we observe today. Therefore, it is difficult to draw conclusions about the connection between the physical conditions in a star-forming region and the resulting period distributions of binaries. All we can say is that in US-A, where we find mainly binaries with small separations, also high-mass stars formed (see Fig. 1). In US-B, however, we find mainly binaries with larger separations and only very few high-mass stars (i. e. B-stars).

The different binary distributions might be the result of the star formation process itself. According to Durisen & Sterzik
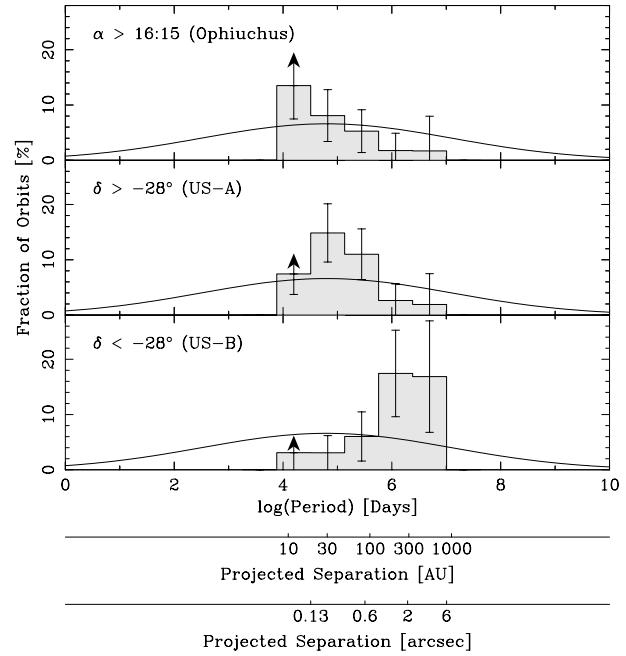
(1994), the parameter space for the formation of binaries depends on the temperature of the molecular cloud. A higher cloud temperature would preferably lead to the formation of closer binaries (Durisen et al. 2000).

The period distributions might also be due to dynamical interaction of the stars. Numerical simulations show that binaries with large separations will be destroyed in dense environments like the Orion Trapezium Cluster, while they can survive in environments like the Taurus-Auriga star-forming region (Kroupa 1995, 1998). This could explain the lack of wide binaries in US-A, especially if this association was smaller and denser in the past. However, it is difficult to explain the deficit of binaries with small separations in US-B with this theory.

5.5. Infrared companions

One of the hypotheses that were proposed to explain the overabundance of binaries in Taurus-Auriga are "Infrared Companions", i. e. companion stars that are relatively bright at infrared wavelengths, but faint in the optical. Since the surveys of young stars are usually performed at $2.2\,\mu$m, while DM91 used optical observations, a large number of infrared companions could explain the different results.

Brandner et al. (1996) surveyed 195 T Tauri stars in the star-forming regions Chamaeleon, Lupus, and Upper Scorpius for binaries. They used seeing-limited images, taken with SUSI (the SUperb Seeing Imager) at the NTT under sub-arcsecond seeing conditions. They used a filter at $1\,\mu$m. The seeing at the time when the observations of stars in Scorpius were done allowed them to resolve binaries with separations down to about $0.7''$.
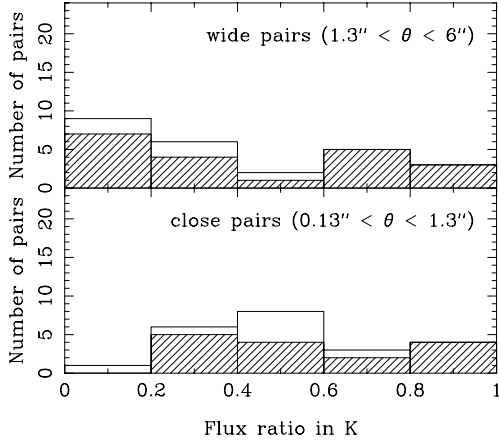
Fig. 13. Distribution of flux ratios for close companions (between $0.13''$ and $1.3''$ or 19 AU and 190 AU separated from the primary) and for distant companions (between $1.3''$ and $6''$ or 190 AU and 870 AU from the primary). The hatched histogram shows the numbers for stars discovered by ROSAT (K99), the open histogram those for stars discovered by EINSTEIN (W94)

In order to minimize chance projections with background stars, they considered only binaries with a separation of less than $3''$.

Wolfgang Brandner kindly provided us with the complete object list, which we compared to our sample. Forty-nine stars were observed in both surveys. All binaries with separations between $0.7''$ and $3''$ that we find have also been discovered by Brandner et al. However, Brandner et al. report a companion to the star RXJ 1545.8-3020 which we do not detect. Re-examination of the SUSI/NTT data shows that the apparent binary companion was an artefact due to telescope movement during the exposure (Neuhäuser & Brandner 1998).

In other words: our survey in the K-band does not find any companions that were missed by Brandner et al. because they are too faint at optical wavelengths. Therefore, Infrared companions cannot explain the high binary fraction among pre-main-sequence objects compared to stars on the main sequence. This apparently disagrees with the results of Ghez et al. (1997), who observed 48 stars in the infrared that have also been observed by Reipurth and Zinnecker (1993) at a wavelength of $0.9\,\mu m$. Ghez et al. discovered two additional companions that were not found by Reipurth and Zinnecker. However, considering the small numbers, this difference is statistically not significant.

5.6. Are the flux ratios of close and wide companions different?

Köhler & Leinert (1998) found a difference in the flux ratio distributions of close ($0.13'' < d < 1.3''$) and wide ($1.3'' < d < 13''$) binaries in Taurus-Auriga: the number of wide pairs increases towards small flux ratios (i. e. faint companions), while the distribution of close pairs is flat with a slight increase towards equal flux ratios. We applied the same test to our binaries in Scorpius-Centaurus, except that the outer limit in separation is $6''$. We decided to use the same dividing line of $1.3''$ between close and wide pairs, since we consider this to be a typical accretion disk radius ($\approx 150 - 200\,\mathrm{AU}$, or $1'' - 1.4''$).

Fig. 13 shows that the distributions are not significantly different. We find at most a slight increase in the number of wide pairs towards small flux ratios, and no preference of close pairs to have equal flux ratios. The lack of close pairs with small flux ratios can easily be explained by our inability to detect faint companions close to the primary. A χ^2 test of the four bins between 0.2 and 1.0 yields a probability of 45 % that both samples were drawn from the same distribution. Given the small number of binaries involved, it is possible that there is a difference between close and wide pairs (as in Taurus-Auriga), which we cannot detect because of statistical noise.

However, it is also possible that the conditions in Scorpius-Centaurus differ from those in Taurus-Auriga. The results for Taurus-Auriga match the predictions of Bate and Bonnell (Bate 1997, Bate & Bonnell 1997), if we take the flux ratios as an approximation for the mass ratios. Bate and Bonnell performed model calculations for accretion from a collapsing cloud onto a protobinary in its center. For a close system, the infalling material has comparatively high angular momentum, which leads to accretion onto the secondary and therefore increases the mass ratio. Of course, this model is not valid if the circumbinary material is removed and the accretion process stopped at an earlier phase of the star-formation process. This is the scenario of the star-formation history in Scorpius-Centaurus proposed by Preibisch and Zinnecker (1999). In their picture, star formation in Upper Scorpius was triggered by the shock wave of a supernova in Upper Centaurus-Lupus. About $1\,\mathrm{Myr}$ later, the star-formation process was halted by the strong winds of the massive stars in Upper Scorpius that dispersed the molecular cloud. This might also have stopped the accretion onto the proto-secondaries, resulting in binaries with smaller mass ratios than in Taurus-Auriga.

5.7. Dependence of multiplicity on spectral type

Fig. 14 shows the multiplicity as function of the spectral type as given in W94 and K99, resp. There is a clear increase of multiplicity towards late-type stars. However, we do not think this effect is real. The sample of stars selected for optical follow-up observations of X-ray sources was flux-limited. Since binaries and multiples are on average brighter than single stars of the same spectral type, one can expect a selection bias similar to the X-ray bias described in Sect. 4.4. The stars with a later spectral type are on average fainter, therefore they should be more affected by this bias.

This effect caused some single stars to be missed in the surveys of W94 and K99 (which affected mostly the results of the last bin in Fig. 14), and therefore an overestimate of the total multiplicity. The total effect on multiplicity probably is small and partly counterbalanced by the use of lower bounds when deriving the total multiplicity (Sect. 5.2). Since the separation and period of a binary have no influence on the brightness of the system, the observed period distributions should not change if we extended our survey to fainter stars. We might have missed some binaries with faint companions, i. e. with small flux ratios.

However, this does not change our conclusions of Sect. 5.3 and 5.6.

6. Summary and conclusions

We carried out a multiplicity survey of 118 X-ray selected T Tauri stars in the Scorpius-Centaurus star-forming region. Our main results are:

— The companion star frequency among the young stars is enhanced by a factor of 1.59 ± 0.34 compared to that of solar-type main-sequence stars.
— The multiplicity of T Tauri stars in Scorpius-Centaurus is slightly lower than in Taurus-Auriga. However, the difference is statistically not significant.
— We find a difference between the distributions of flux ratios: There are more binaries with nearly equal brightness in Taurus-Auriga than in Scorpius-Centaurus.
— The period distributions of binaries in the two subgroups Upper Scorpius A and B are different: The peak of the distribution of stars in US-A is at about 10^5 days (corresponding to $\approx 50\,\mathrm{AU}$), while that of stars in US-B is around $10^{6.5}$ days ($350\,\mathrm{AU}$).
— We find no evidence for a significant number of infrared companions. We conclude that they can't explain the over-abundance of binaries among young stars.
— The flux ratio distributions of close ($0.13'' < d < 1.3''$) and wide ($1.3'' < d < 6''$) binaries show no significant difference. This is in contrast to the stars in Taurus-Auriga, where the number of wide pairs increases towards systems with faint companions, while close pairs tend to have equal flux ratios. This might indicate that the accretion process onto proto-binaries in ScoCen was abruptly halted.

We conclude that the multiplicity of young low-mass stars in the OB association Scorpius-Centaurus is nearly as high as in the T association Taurus-Auriga, and is higher than that of main-sequence field-stars or young low-mass stars in dense clusters. However, there are also some differences between binaries in Taurus-Auriga and Scorpius-Centaurus that are probably related to the physical conditions in the star-forming regions.

The difference between the period distributions in Upper Scorpius A and B shows that the shape of the orbital period distribution is not an universal quantity that is the same in each star-forming region. The shape of the period distribution might be the result of the environmental conditions during the star-formation process and/or dynamical interactions of the stars afterwards. In particular, the lack of wide binaries in Upper Scorpius A can be explained by dynamical interactions if this subgroup was born as a much denser concentration. Further work, both theoretical and observational, is required to explore the influence of the environment on binary formation and evolution.
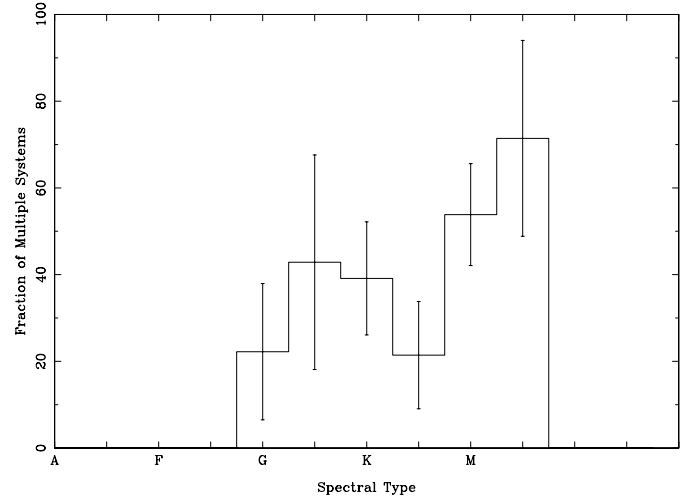
Fig. 14. Multiplicity as function of the spectral type

Appendix A: A brief introduction to speckle interferometry

The Earth's atmosphere blurs the images we obtain of celestial objects, limiting the resolution of conventional imaging to $\approx 1''$. Mathematically, this process can be described as the convolution of the intrinsic object brightness distribution $O(\boldsymbol{x})$ with the point-spread function $P(\boldsymbol{x})$:

$$I(\boldsymbol{x}) = \int O(\boldsymbol{x}') \cdot P(\boldsymbol{x} - \boldsymbol{x}')\,\mathrm{d}\boldsymbol{x}'.$$

The fourier-transformed equivalent of this equation is a simple multiplication:

$$\tilde{I}(\boldsymbol{u}) = \tilde{O}(\boldsymbol{u}) \cdot \tilde{P}(\boldsymbol{u}),$$

where tildes denote quantities in Fourier-space, and $\boldsymbol{u}$ is a point in the spatial frequency plane.

In order to retain the information about high spatial frequencies in the object brightness distribution, we have to use integration times of the order of the coherence time of the atmosphere, which is about $100\,\mathrm{ms}$ at near-infrared wavelengths. To obtain a reasonable signal-to-noise ratio, one takes some 500 to 1000 images of one object. It is not useful to simply average these images, since this would result in the low resolution of a long-exposure image. Instead, Labeyrie's (1970) method is based on averaging the power spectrum $|\tilde{I}(\boldsymbol{u})|^2$:

$$\left\langle |\tilde{I}(\boldsymbol{u})|^2 \right\rangle = |\tilde{O}(\boldsymbol{u})|^2 \cdot \left\langle |\tilde{P}(\boldsymbol{u})|^2 \right\rangle.$$

Here, we made use of the assumption that the object brightness distribution does not change during the observation. This equation can be used to compute $|\tilde{O}(\boldsymbol{u})|^2$ if the point-spread function is known.

An estimate for the point-spread function can be obtained from observations of a point source, the so-called reference star. This reference star has to be located sufficiently close to the object ($\approx 1°$), and the observation has to be carried out within a few minutes before or after the observation of the object to be useful for the deconvolution process.

Then, the power spectrum of the object brightness distribution can be computed from the observed power spectra:

$$|\tilde{O}(\boldsymbol{u})|^2 = \frac{\left\langle |\tilde{I}_{\mathrm{Obj}}(\boldsymbol{u})|^2 \right\rangle}{\left\langle |\tilde{I}_{\mathrm{Ref}}(\boldsymbol{u})|^2 \right\rangle} \,,$$

where Obj and Ref denote the observations of the object and reference star. The result improves further if one subtracts noise terms from the object and reference measurements before the division.

However, this gives us only the modulus of the object brightness distribution. In order to reconstruct the full image of the object, we need the phase of the complex visibility. In this work, we use two different methods: the Knox-Thompson algorithm (Knox & Thompson 1974), and an algorithm based on the bispectrum (Lohmann et al. 1983).

Knox and Thompson (1974) proposed to average the crossspectrum of the short-exposure images:

$$\left\langle \tilde{I}(\boldsymbol{u}_1) \cdot \tilde{I}^*(\boldsymbol{u}_2) \right\rangle$$
$$= |\tilde{I}(\boldsymbol{u}_1)| \cdot |\tilde{I}(\boldsymbol{u}_2)| \cdot \mathrm{e}^{i(\varphi(\boldsymbol{u}_1)-\varphi(\boldsymbol{u}_2)+\psi(\boldsymbol{u}_1)-\psi(\boldsymbol{u}_2))},$$

where $\varphi(\boldsymbol{u})$ is the phase of the true object brightness distribution, and $\psi(\boldsymbol{u})$ is the distortion caused by the atmosphere. If the points $\boldsymbol{u}_1$ and $\boldsymbol{u}_2$ are sufficiently close to each other, the distortions cancel to good accuracy, and we can use this relation to obtain the phase difference between two neighbouring spatial frequency points. Since the object brightness distribution is a real quantity, the phase of its fourier transform is antisymmetric ($\varphi(\boldsymbol{u}) = -\varphi(-\boldsymbol{u})$) and therefore $\varphi(0) = 0$. With this starting point, one can recursively build up the phases at all points of the image.

Another way to reconstruct the phase is based on the bispectrum $\tilde{B}(\boldsymbol{u}_1, \boldsymbol{u}_2)$, which is defined as

$$\tilde{B}(\boldsymbol{u}_1, \boldsymbol{u}_2) = \left\langle \tilde{I}(\boldsymbol{u}_1) \cdot \tilde{I}(\boldsymbol{u}_2) \cdot \tilde{I}^*(\boldsymbol{u}_1 + \boldsymbol{u}_2) \right\rangle .$$

Division by the bispectrum obtained from images of the reference star yields the bispectrum of the true object brightness distribution. Its phase $\beta(\boldsymbol{u}_1, \boldsymbol{u}_2)$ gives a relation between different points in the phase image:

$$\beta(\boldsymbol{u}_1, \boldsymbol{u}_2) = \varphi(\boldsymbol{u}_1) + \varphi(\boldsymbol{u}_2) - \varphi(\boldsymbol{u}_1 + \boldsymbol{u}_2).$$

This relation can also be used to recursively reconstruct the full phase image. Since usually more than one pair of points $\boldsymbol{u}_1$, $\boldsymbol{u}_2$ may be used to compute $\varphi(\boldsymbol{u}_1 + \boldsymbol{u}_2)$, one can average the results. Therefore, the phase obtained from this method usually has a better signal-to-noise ratio than that based on the Knox-Thompson algorithm. However, we prefer to use both methods and compare the results in order to obtain a more reliable estimate of the binary parameters.

References

Bate M.R., 1997, MNRAS 285, 16

Bate M.R., Bonnell I.A., 1997, MNRAS 285, 33

Bouvier J., Rigaut F., Nadeau D., 1997, A&A 323, 139

Brandner W., Alcalá J.M., Kunkel M., Moneti A., Zinnecker H., 1996, A&A 307, 121

Brandner W., Köhler R., 1998, ApJ 499, L79

Duquennoy A., Mayor M., 1991, A&A 248, 455

Durisen R.H., Sterzik M.F., 1994, A&A 286, 84

Durisen R.H., Sterzik M.F., et al., 2000, in prep.

Fischer D.A., Marcy G.W., 1992, ApJ 396, 178

Frink S., 1999, Ph.D. Thesis, Universität Heidelberg

Ghez A.M., Neugebauer G., Matthews K., 1993, AJ 106, 2005

Ghez A.M., McCarthy D.W., Patience J., Beck T., 1997, AJ 481, 378

Henry T.J., McCarthy D.W., 1993, AJ 106, 773

Hofmann R., Blietz M., Duhoux Ph., Eckart A., Krabbe A., Rotaciuc V., 1992, In: Ulrich M.-H. (ed.) Progress in Telescope und Instrumentation Technologies, ESO Conference and Workshop Proceedings No. 42, p. 617

Knox K.T., Thompson B.J., 1974, ApJ 193, L45

Köhler R., Leinert Ch., 1998, A&A 331, 977

Kroupa P., 1995, MNRAS 277, 1491

Kroupa P., 1998, MNRAS 298, 231

Kunkel M., 1999, Ph.D. Thesis, Julius-Maximilians-Universität Würzburg (K99)

Kunkel M., Brandner W., Yorke H.W., et al., 2000, in prep.

Labeyrie A., 1970, A&A 6, 85

Leinert Ch., 1992, In: Ray T.P., Beckwith S. (eds.) Star Formation and Techniques in Infrared and mm-Wave Astronomy. Proceedings of the European Astrophysical Doctoral Network Summer School V, Lecture Notes in Physics, Springer Verlag, Berlin, Heidelberg, New York

Leinert Ch., Henry T., Glindemann A., McCarthy D.W., 1997, A&A 325, 159

Leinert Ch., Zinnecker H., Weitzel N., et al., 1993, A&A 278, 129

Lohmann A.W., Weigelt G., Wirnitzer B., 1983, Appl. Opt. 22, 4028

Mayor M., Duquennoy A., Halbwachs J.-L., Mermilliod J.-C., 1992, In: McAlister H.A., Hartkopf W.I. (eds.) Complementary Approaches to Double and Multiple Star Research. IAU Colloquium 135, San Francisco, p. 73

Miller G.E., Scalo J.M., 1978, PASP 90, 506

Neuhäuser R., Brandner W., 1998, A&A 330, L29

Padgett D.L., Strom S.E., Ghez A., 1997, ApJ 477, 705

Patience J., Ghez A.M., Reid I.N., Weinberger A.J., Matthews K., 1998, AJ 115, 1972

Petr M.G., Coudé du Foresto V., Beckwith S.V.W., Richichi A., McCaughrean M.J., 1998, ApJ 500, 825

Preibisch Th., Guenther E., Zinnecker H., et al., 1998, A&A 333, 619

Preibisch Th., Zinnecker H., 1999, AJ 117, 2381

Press W.H., Teukolsky S.A., Vetterling W.T., Flannery B.P., 1994, Numerical Recipes in C. 2nd Ed., Cambridge University Press

Prosser C.F., Stauffer J.R., Hartmann L., et al., 1994, ApJ 421, 517

Reipurth B., Zinnecker H., 1993, A&A 278, 81

Richichi A., Köhler R., Woitas J., Leinert Ch., 1999, A&A 346, 501

Simon M., Close L.M., Beck T.L., 1999, AJ 117, 1375

Simon M., Chen W.P., Howell R.R., Benson J.A., Slowik D., 1992, ApJ 384, 212

Simon M., Ghez A.M., Leinert Ch., et al., 1995, ApJ 443, 625

Walter F.M., Vrba F.J., Mathieu R.D., Brown A., Myers P.C., 1994, AJ 107, 692 (W94)

de Zeeuw P.T., Hoogerwerf R., de Bruijne J.H.J., Brown A.G.A., Blaauw A., 1999, AJ 117, 354

de Zeeuw P.T., Brown A.G.A., de Bruijne J.H.J., et al., 1998, In: HIPPARCOS Venice '97 Symposium, ESA SP-402

Zinnecker H., Brandner W., Reipurth B., 1992, In: McAlister H.A., Hartkopf W.I. (eds.) Complementary Approaches to Double and Multiple Star Research. IAU Colloquium 135, San Francisco, p. 50